Hydrogen Transfer Reaction in Polycyclic Aromatic Hydrocarbon Radicals

ARTICLE *in* THE JOURNAL OF PHYSICAL CHEMISTRY A · JUNE 2014

Impact Factor: 2.69 · DOI: 10.1021/jp503872m · Source: PubMed

4 AUTHORS, INCLUDING:

Liuming Yan
Shanghai University
66 PUBLICATIONS **832** CITATIONS

SEE PROFILE

THE JOURNAL OF PHYSICAL CHEMISTRY A

Article

pubs.acs.org/JPCA

Hydrogen Transfer Reaction in Polycyclic Aromatic Hydrocarbon Radicals

Huiting Liu,[†] Liuming Yan,*[,†] Baohua Yue,[†] and Aijun Li[‡]

[†]Department of Chemistry, Innovative Drug Research Center, College of Sciences [‡] Research Center for Composite Materials Shanghai University, 99 Shangda Road, Shanghai 200444, China

Supporting Information

ABSTRACT: Density functional theory calculations have been successfully applied to investigate the formation of hydrocarbon radicals and hydrogen transfer pathways related to the chemical vapor infiltration process based on model molecules of phenanthrene, anthra[2,1,9,8-*opqra*]tetracene, dibenzo[*a*,*ghi*]perylene, benzo[*uv*]-naphtho[2,1,8,7-*defg*]pentaphene, and dibenzo[*bc*,*ef*]ovalene. The hydrogen transfer reaction rate constants are calculated within the framework of the Rice–Ramsperger–Kassel–Marcus theory and the transition state theory by use of the density functional theory calculation results as input. From these calculations, it is concluded that the hydrogen transfer reaction between two bay sites can happen almost spontaneously with energy barrier as low as about 4.0 kcal mol^{-1}, and the hydrogen transfer reactions between two armchair sites possess lower energy barrier than those between two zigzag sites.

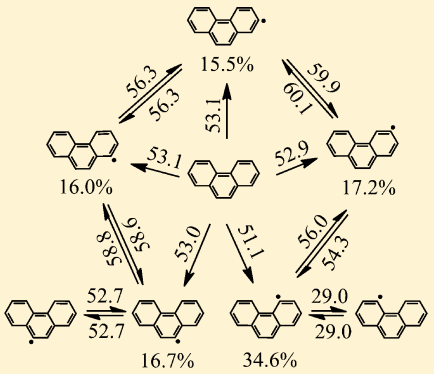

1. INTRODUCTION

Carbon/carbon (C/C) composite materials have been widely applied to the aeronautical, aerospace, medical, and automotive industries owing to their low density and swell factor, high specific modulus, excellent environmental stability, and antifrictional and antithermal shock characteristics.[1−5] The vast potential application fields and the great demand for high-quality C/C composite materials have attracted numerous research groups to optimize their synthesizing process in the past years.[6−10] Among the many synthesizing methods, the chemical vapor infiltration (CVI) has stood out as one of the most accepted processes to grow pyrolytic C/C composite materials.[11−15] The advantages of the CVI process include its low operational temperature, large obtainable products, and the ease of transferring products onto other substrates for further processing. However, the quality of the products depends on the process temperature,[16−19] pressure,[20,21] specific surface area,[22−24] and homogeneous (heterogeneous) reaction dynamics in the gas phase (on the surface).[25]

In order to clarify the molecular mechanism of the CVI processes, tens of pathways, including the elementary reactions and their corresponding rate constants, were proposed.[8,26−31] The most widely accepted pathway is the hydrogen abstraction-C_2H_2 addition (HACA) mechanism,[32,33] where the second aromatic ring is formed via the HACA sequence involving a single-activation-repetitive-acetylene-addition pathway as proposed by Bittner and Howard[34] and a repetitive-activation-acetylene-addition sequence.[35] The HACA mechanism involves a high abundance of acetylene and benzene/phenyl in the combustion flame.[36] However, the HACA mechanism is supposed to be too slow to compete with the very fast process of polycyclic aromatic hydrocarbons (PAHs) formation, as the mass of product species increases only 24 Da in each step.[32] Therefore, the aromatic ring−ring condensation and acetylene addition mechanism or aryl−aryl combination followed by H_2-elimination and ring cyclization was proposed.[32] In a recent paper, Shukla and Koshi proposed a phenyl addition cyclization (PAC) mechanism because of its efficiency to continue the endless growth of PAHs, while the HACA was only found efficient for producing symmetrical PAHs by filling a triple fusing site (the four carbon bay structure).[37]

Kinetic modeling and molecular simulations have been an important methodology in the optimization of pyrolytic carbon materials.[38−41] And in the bottom of any kinetic modeling there is the chemical reaction rate constants as the most essential parameters for the numerical simulations. Though modern experimental technologies have allowed the accurate determination of chemical reaction rate constants, the complexity of CVI pathways has hindered the determination of such data. On the other hand, ab initio calculations, especially the density functional theory (DFT) calculations, have stood out as an essential and indispensible method to calculate chemical reaction rate constants owing to the great success of modern computing technology and computational programs. For example, Wodrich et al. calculated the accurate thermochemistry of hydrocarbon radicals via an extended generalized bond separation reaction scheme.[42] Furthermore, the chemical reaction rate constants could be evaluated in terms of conventional transition state theory (TST) combined with the Rice-Ramsperger-Kassel-Marcus (RRKM) theory based on

Received: April 21, 2014
Revised: June 3, 2014
Published: June 3, 2014

ab initio energies of stationary and transition states of the chemical reactions.[32,36,43] On the basis of such approach, Kislov et al. calculated the reaction rate of the phenyl radical with propylene[43] and of naphthalene with C_2H_2 forming various three-fused aromatic rings.[36]

In a CVI process, no matter how the precursor molecules are produced and new carbon moieties are added to the existing precursor molecules, the structure and morphology of the final C/C composite material depends not only on what kind of carbon moieties are added but also on the position of precursor molecules on which the carbon moieties are added. The formation of active sites on precursor molecules, or the formation of radicals, is the initiating step of a series radical additions to the growing precursor molecules. And the rearrangements of active sites, or the hydrogen transfer reactions, compete with the addition reactions to the growing precursor molecules. Therefore, it is essentially important to determine the relative stabilities of various radicals and the hydrogen transfer reaction rates between various sites to optimize the structure and morphology of the final C/C composite products.

In this work, we will study the stabilities of various radicals and the hydrogen transfer reactions in terms of transition states (TS) and energy barriers of various possible reaction pathways using DFT calculations. In addition, reaction rate constants and activation energies will be calculated by use of conventional TST combined with the RRKM theory.

2. COMPUTATIONAL METHODS

2.1. Model Molecules and Their Labeling. The pyrolytic process of hydrocarbons can be characterized by a series of radical reactions including dissociation (the formation of radicals), hydrogen transfer reaction (the isomerization of radicals), radical addition (the growth of radicals), and radical termination. The formation of radicals and hydrogen transfer reaction are two of the determining steps influencing the structure and morphology of the final product. In the present work, a couple of model molecules and corresponding radicals, including phenanthrene (PHE), anthra[2,1,9,8-*opqra*]tetracene (ATA), dibenzo[*a*,*ghi*]perylene (DBP), benzo[*uv*]naphtho-[2,1,8,7-*defg*]pentaphene (BNP), and dibenzo[*bc*,*ef*]ovalene (DBO) (Scheme 1), and various radicals derived, will be studied in terms of their relative stabilities and isomerization reactivity. These model molecules represent the typical edge structures of polycyclic aromatic hydrocarbons, including zigzag, armchair, and bay configurations, and the relative stabilities and reactivity of the derived radicals can be applied to predict the characteristics of pyrolytic carbon.

If a radical is derived from the PHE by elimination of a hydrogen atom at the 1-position, the radical will be named as phenanthr-1-yl (PHE-1-yl). The hydrogen transfer pathway from the 1-position to the 2-position (a hydrogen atom transfers from the 1-position to the 2-position) will be named as HT(1 > 2), and the corresponding transition state will be named as TS(1 ≠ 2). This nomenclature is applied to the other model molecules, radicals, hydrogen transfer pathways, and transition states.

Scheme 1. Numbering of (a) PHE, (b) ATA, (c) DBP, (d) BNP, and (e) DBO

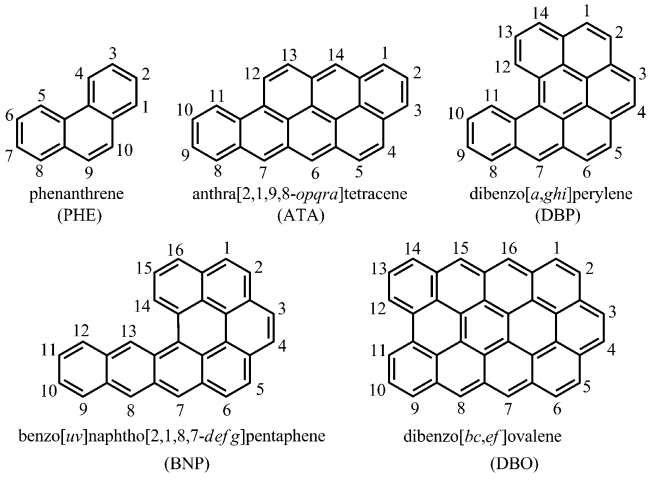

2.2. Ab initio Calculations. In order to select an adequate basis set for the ab initio calculations, the geometries and energies of hydrogen transfer pathway of phenanthryl (Figure 1), including stationary reactant PHE-4-yl, product PHE-3-yl, and transition state TS(4 ≠ 3), are studied at various levels of theory as implemented in GAUSSIAN 03.[44] The geometrical optimizations are conducted using the DFT approach based on the B3LYP, B3PW91, MPW1PW91, and PBE1PBE functionals. By enlarging the basis set from 6-31G(D) to 6-311G(D), 6-311G(D,P), 6-311+G(D,P), and 6-311++G(D,P), the geometry and the energy gradually converge at theory level of B3LYP/6-311+G(D,P) as summarized in Table 1. Considering both the computational accuracy and efficiency, all the following calculations are conducted according to the following steps: geometrical optimization and frequency calculation at B3LYP/6-311+G(D,P) level of theory and zero-point energy (ZPE) and thermal correction based on the B3LYP/6-311+G(D,P) frequencies.

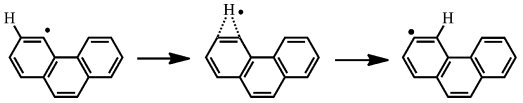

Figure 1. Hydrogen transfer pathway used for the basis set optimization.

The energy of a gas molecule at temperature T will be evaluated as,

$$E_T = E_{\mathrm{B3LYP}} + E_{\mathrm{ZPE}} + E_{\mathrm{thermal}} \quad (1)$$

where E_{B3LYP}, E_{ZPE}, and E_{thermal} are B3LYP/6-311+G(D,P) energy, zero-point energy, and thermal correction to the energy at temperature T. The enthalpy of a gas molecule will be evaluated as,

$$H_T = E_{\mathrm{B3LYP}} + E_{\mathrm{ZPE}} + H_{\mathrm{thermal}} \quad (2)$$

where H_{thermal} is thermal correction to the enthalpy at temperature T. The Gibbs free energy of a gas molecule will be evaluated as,

$$G_T = E_{\mathrm{B3LYP}} + E_{\mathrm{ZPE}} + G_{\mathrm{thermal}} \quad (3)$$

where G_{thermal} is thermal correction to the Gibbs free energy at temperature T. And the standard formation enthalpy of a hydrocarbon molecule C_nH_m is evaluated as,

$$\Delta_f H_T^{\theta}[C_nH_m] = H_T[C_nH_m] - n(H_T[C] - \Delta H_{\mathrm{vap},T}^{\theta}[C]) - 0.5mH_T[H_2] \quad (4)$$

dx.doi.org/10.1021/jp503872m | J. Phys. Chem. A 2014, 118, 4405−4414

Table 1. Comparison of Total Energy, E_T (in Hartree), and Activation Energy, E_a (in kcal mol^{-1}), Evaluated at Various Levels of Theory[a]

	PHE-4-yl	TS(4 ≠ 3)	PHE-3-yl	E_a
		B3LYP		
6-31G(D)	−538.481 07	−538.375 55	−538.490 60	66.21
6-311G(D)	−538.590 23	−538.486 40	−538.599 60	65.16
6-311G(D,P)	−538.606 19	−538.504 22	−538.615 67	63.99
6-311+G(D,P)	−538.611 64	−538.509 98	−538.621 29	63.79
6-311++G(D,P)	−538.611 73	−538.510 10	−538.621 38	63.77
		B3PW91		
6-31G(D)	−538.274 41	−538.181 93	−538.271 53	58.03
6-311G(D)	−538.373 07	−538.282 12	−538.370 18	57.07
6-311G(D,P)	−538.389 02	−538.300 23	−538.386 26	55.71
6-311+G(D,P)	−538.394 03	−538.305 60	−538.391 30	55.49
6-311++G(D,P)	−538.394 26	−538.305 84	−538.391 53	55.48
		MPW1PW91		
6-31G(D)	−538.356 80	−538.263 00	−538.354 04	58.86
6-311G(D)	−538.454 69	−538.362 52	−538.451 95	57.84
6-311G(D,P)	−538.470 73	−538.380 76	−538.468 10	56.46
6-311+G(D,P)	−538.476 15	−538.386 58	−538.473 56	56.21
6-311++G(D,P)	−538.476 39	−538.386 83	−538.473 79	56.20
		PBE1PBE		
6-31G(D)	−537.842 81	−537.749 80	−537.840 18	58.36
6-311G(D)	−537.938 62	−537.847 28	−537.935 98	57.32
6-311G(D,P)	−537.954 76	−537.865 68	−537.952 24	55.90
6-311+G(D,P)	−537.960 24	−537.871 56	−537.957 76	55.65
6-311++G(D,P)	−537.960 47	−537.871 80	−537.957 99	55.64

[a]All the energies are corrected by the zero-point energies and thermal energies at 298.15 K.

where $H_T[C_nH_m]$, $H_T[C]$, $H_T[H_2]$ are enthalpies for molecule C_nH_m, atom C, and molecule H_2 at the gaseous state as evaluated from eq 2, and $\Delta H^{\theta}_{vap,T}[C]$ is the experimental vaporization enthalpy of graphite at standard state with a value of 171.45 kcal mol^{-1} (at 298.15 K).[45]

The internal reaction coordination (IRC) is evaluated as the hydrogen transfer pathway which connects stationary reactant, transition state, and stationary product on the potential energy surface. The population probability of a radical R, $p_T[R]$, is evaluated using the Boltzmann distribution function,

$$p_T[R] = g[R]\exp(-\Delta E_T[R]/k_BT)/\sum_i g[i]\exp(-\Delta E_T[i]/k_BT) \quad (5)$$

where $\Delta E_T[i]$ is energy relative to the ground state, $g[i]$ is the degeneracy, k_B is the Boltzmann constant, T is the temperature, and the summation runs over all the possible radicals of the same molecule.

2.3. Calculation of Reaction Rate Constants. The hydrogen transfer reaction rate constants are calculated by use of the ChemRate program.[46] The ChemRate program evaluates rate constant of unimolecular reaction based on the RRKM theory and the TST theory,

$$k(\varepsilon) = l^+\frac{G^+(\varepsilon)}{hN(\varepsilon + \varepsilon_0)} \quad (6)$$

where $G^+(\varepsilon)$ is the total number of states of the transition state, up to and including ε, l^+ is the reaction path degeneracy, $N(\varepsilon + \varepsilon_0)$ is density of states, and h is the Planck constant.

During the calculation of hydrogen transfer reaction-rate constant, the energies and frequencies evaluated by B3LYP/6-311+G(D,P) are used. The energy transfer is modeled using the master equation with argon as buffer gas, and 3.47 Å and 114.0 K are used for the Lennard-Jones collision diameter and attraction energy.[43]

3. CALCULATION RESULTS

3.1. PHE. *3.1.1. Formation of Radicals.* The radical isomers, PHE-1-yl, PHE-2-yl, PHE-3-yl, PHE-4-yl, and PHE-10-yl, as well as their formation of energies and population probabilities, are summarized in Figure 2. Among these radicals, the PHE-1-yl and PHE-10-yl represent radicals at the zigzag edge and PHE-4-yl the radical at the armchair edge, and PHE-

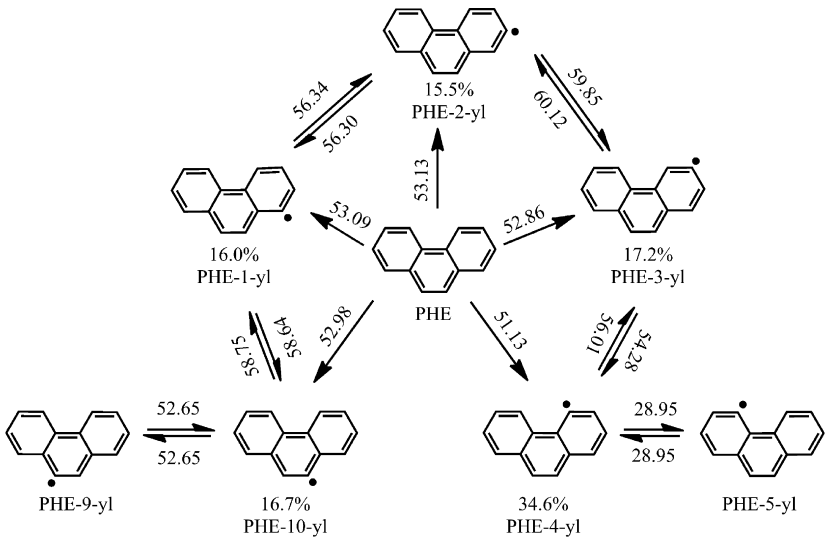

Figure 2. Formation of radicals and hydrogen transfer pathways of PHE. The numbers beside the one-way arrows and the reversible arrows are formation energies and energy barriers, respectively, the numbers below the radicals are population probabilities at 1273.15 K, and the unit for energies is kcal mol^{-1} (noticing that the same symbols are applied to Figures 7, 9, and 11).

dx.doi.org/10.1021/jp503872m | J. Phys. Chem. A 2014, 118, 4405−4414

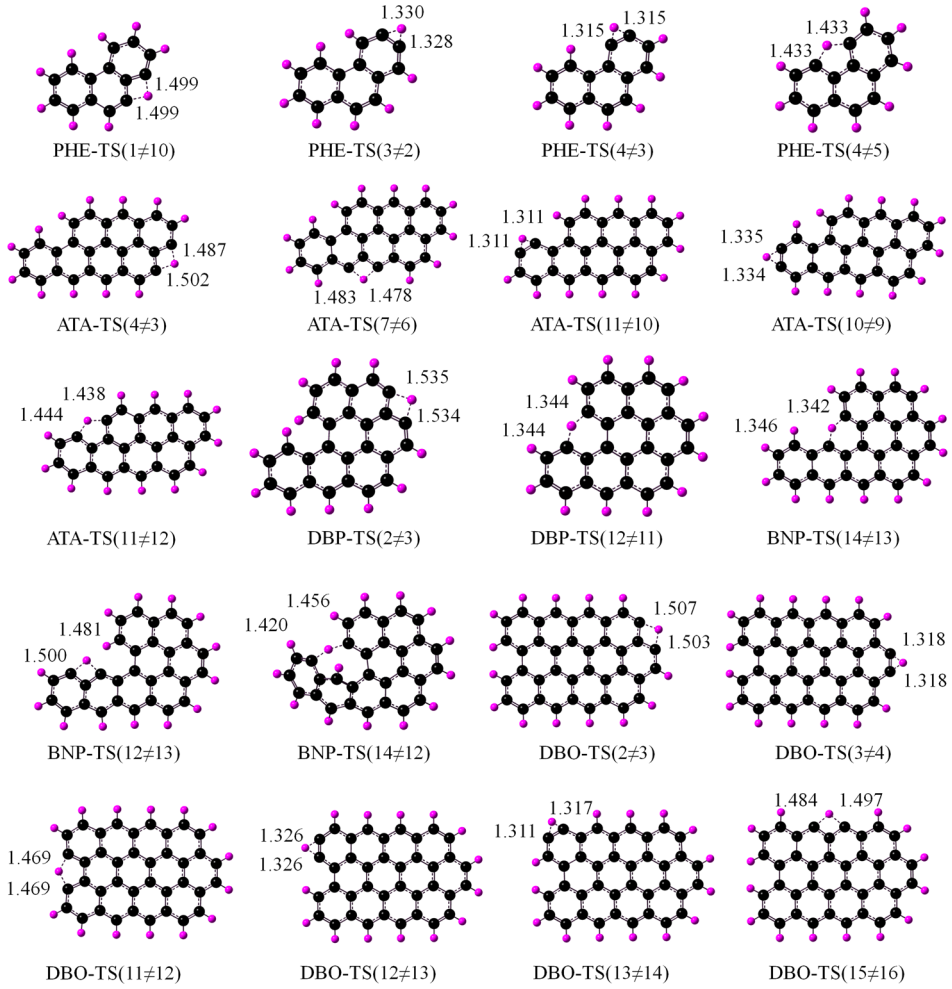

Figure 3. Typical structures of transition states (the numbers are C−H distance in angstroms).

2-yl and PHE-3-yl the radicals at the corner of a zigzag edge and a armchair edge. From Figure 2, it could be seen that the most stable radical is the PHE-4-yl at the armchair edge, and the other radicals at the zigzag edge or the corner are slightly unstable compared with the radicals at the armchair edge from 1.73 to 2.00 kcal mol^{-1}. Therefore, it could be concluded that the armchair edges are more reactive than the zigzag edges and the corners.

In addition, the minor differences in formation energies of these radicals cause significant changes in their population probabilities. At 1273.15 K, the most stable radical PHE-4-yl possesses a population probability of 34.6%, while the other radicals possess population probabilities from 15.5% to 17.2%. And at 298.15 K, the PHE-4-yl possesses a population probability of 85.5%, compared with population probabilities from 2.9% to 4.7% of the other radicals. Therefore, the edges of pyrolytic carbon materials can be controlled by processing temperature: the armchair edges are dominant growth edges at low temperature attributing to their relatively higher population probabilities, while this dominancy is unobvious at high temperatue because the differences in population probabilities of different edges are not obvious.

3.1.2. Hydrogen Transfer Pathways. The hydrogen transfer pathways, or hydrogen transfer reactions, of the PHE radicals are also summarized in Figure 2. There are six hydrogen transfer pathways including HT(4 > 3), HT(3 > 2), HT(2 > 1), HT(1 > 10), HT(4 > 5), and HT(9 > 10), and the hydrogen transfer pathways HT(4 > 5) and HT(9 > 10) do not result in any changes in radicals because of the structural symmetry of PHE. As reported in the previous section, the formation energies of radicals at different edges differ only slightly for 2.00 kcal mol^{-1} in maximum, however, the hydrogen transfer reaction energy barriers, the energy difference between a transition state and its corresponding reactant, show great variation among different hydrogen transfer pathways. The HT(2 > 3) and HT(3 > 2) pathways, hydrogen transfer between two corner sites, possess greatest energy barriers at 60.12 and 59.85 kcal mol^{-1}, and the pathways between two zigzag sites, the HT(1 > 10) and HT(10 > 1) pathways, possess slightly lower energy barriers at 58.75 and 58.64 kcal mol^{-1}. However, the hydrogen transfer pathways between a corner site and an edge site (zigzag edge or armchair edge) possess still lower energy barriers, ranging from 54.28 to 56.34 kcal mol^{-1}. Finally, the hydrogen transfer between armchair sites, the HT(4 > 5) or HT(5 > 4) pathways, possess a much lower energy barrier at 28.95 kcal mol^{-1}. Evidently, the overall energy barriers differ much greater than the formation energies, and the hydrogen transfer pathways between two armchair sites possesses the lowest-energy barrier.

3.1.3. Transition States and Internal Reaction Coordinates. For all the transition states of TS($\alpha \neq \beta$), where the α and β represent two carbon atoms between which the hydrogen atom transfers, the C_α−H and C_β−H distances are almost equivalent (Figure 3). However, the spatial structures of the

dx.doi.org/10.1021/jp503872m | J. Phys. Chem. A 2014, 118, 4405−4414

transition states show quite different characteristics: transition states of hydrogen transfer pathways between two bonded carbon atoms, including TS(4 ≠ 3), TS(2 ≠ 3), and TS(1 ≠ 2), are nonplanar with the hydrogen atom above or below the molecular plane, while those of hydrogen transfer between two zigzag sites or armchair site carbon atoms (nonbonded carbon atoms) are coplanar.

For transition states of hydrogen transfer between two bonded carbon atoms, the C−H distances vary from 1.306 to 1.330 Å, while those between two zigzag site carbon atoms separated by one carbon atom, the C−H distances increase to about 1.499 Å, indicating a longer distance to be traveled by the transferring hydrogen atom. The C−H distances in the TS(4 ≠ 5), where the hydrogen transfers between two armchair carbon atoms separated by two carbon atoms, are 1.433 Å, in the intermediate of these three cases.

In Figure 4, it shows three internal reaction coordinates (IRC) for hydrogen transfer between carbon atoms separated by zero, one, and two carbon atoms. The relative energy along IRC is evaluated relative to the reactant. These IRCs confirm that all the transition states are saddle points connecting the correct reactants and products.

For the hydrogen transfer between two bonded carbon atoms, the hydrogen atom will leave the molecular plane and reach a maximum dihedral angle of 11.14° at the transition state as shown in Figure 5. After reaching the transition state, the hydrogen atom will come back as the dihedral angle gradual decreases, and the product is resulted. However, for the hydrogen transfer between zigzag site or armchair site carbon atoms separated by one or two carbon atoms, the hydrogen atom will never leave the molecular plane and the IRC is coplanar.

3.1.4. Hydrogen Transfer Reaction Rate Constants. The high-pressure hydrogen transfer reaction rate constants are calculated using the RRKM/TST approach based on B3LYP/6-311+G(D,P) energies and vibrational frequencies. The reaction rate constants of the six hydrogen transfer pathways within temperature range from 300 to 3000 K are summarized in Table SI-2 of the Supporting Information. The reaction rate constants are negligible at low temperature, however, increase quickly with temperature. At about 1000 K, the hydrogen transfer reactions are comparable with the pyrolytic reactions of hydrocarbons.[47] As the temperature increases to 3000 K, the reaction rate constants even increase to as high as 10^{10} s^{-1}, which are among the fastest chemical reaction rate constants.

By fitting the hydrogen transfer reaction rate constants to the Arrhenius equation,

$$k = A(T/T_0)^n \exp(-E_a/RT) \quad (7)$$

where T_0 = 298.15 K, and the preexponential factor A, activation energy E_a, and temperature correction coefficient n are obtained. In this work, the temperature correction coefficient is fixed at 0.5 because the fitted value varies only slightly above 0.5. From Figure 6, it could be concluded that excellent linear relationship exists between the logarithm of rate constant and the reciprocal of temperature. From Table 2, it could be seen that all the reactions have similar pre-exponential parameters at about 10^{13} s^{-1} but very different activation energies. Among the six hydrogen transfer pathways, the HT(4 > 5) pathway between two armchair site carbon atoms has the lowest activation energy at 32.8 kcal mol^{-1} and the HT(3 > 2) pathway between two corner site carbon atoms the highest activation energy at 64.9 kcal mol^{-1}.

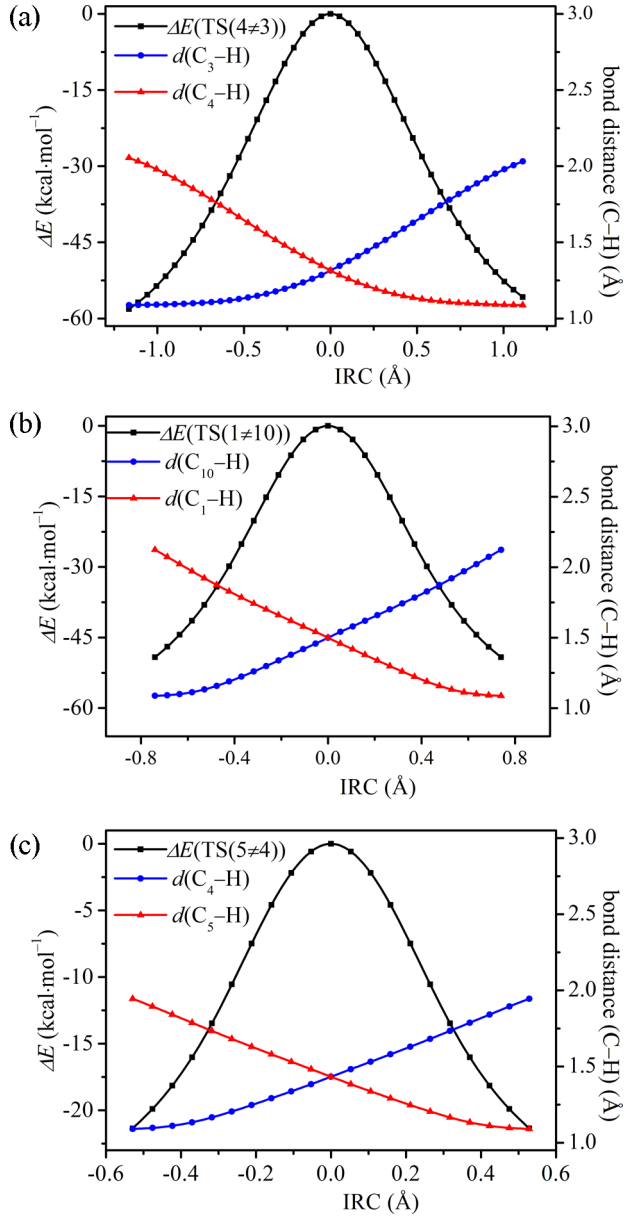

Figure 4. Relative energies and C−H distances of hydrogen transfer pathways along IRC: (a) HT(4 > 3), (b) HT(1 > 10), and (c) HT(5 > 4).

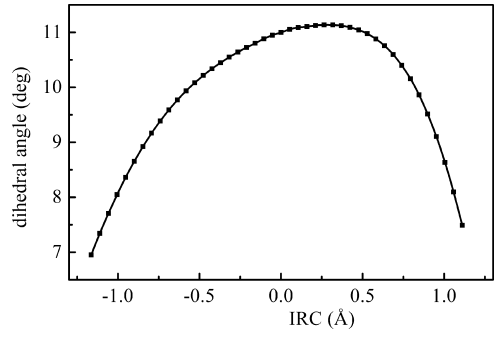

Figure 5. Dihedral angle of the HT(4 > 3) pathway along the IRC.

From these calculations, it could be concluded that hydrogen transfer pathway between two armchair carbon atoms is the fastest, that between two corner site carbon atoms is the

dx.doi.org/10.1021/jp503872m | J. Phys. Chem. A 2014, 118, 4405−4414

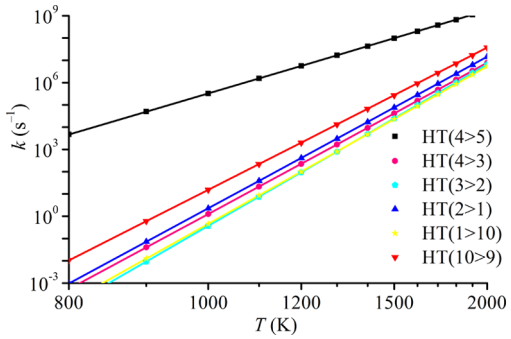

Figure 6. Hydrogen transfer reaction rate constants of the PHE radicals.

Table 2. Activation Energies, E_a (kcal mol^{-1}), and Preexponential Factors, A (s^{-1}), for the Hydrogen Transfer Reactions of Various Radicals and Members-in-Ring (m) for Their Corresponding Transition States

reactions	m	log A	E_a	reactions	m	log A	E_a
PHE				**DBP**			
HT(4 > 5)	5	12.4	32.8	HT(12 > 11)	6	12.2	7.5
HT(4 > 3)	3	13.1	60.7	HT(2 > 3)	4	13.4	68.7
HT(3 > 2)	3	13.5	64.9	**BNP**			
HT(2 > 1)	3	13.4	60.8	HT(14 > 12)	8	11.4	75.3
HT(1 > 10)	4	13.2	63.2	HT(14 > 13)	6	12.2	7.5
HT(10 > 9)	3	13.4	57.0	HT(12 > 13)	4	13.6	60.3
ATA				**DBO**			
HT(11 > 12)	5	12.8	33.2	HT(11 > 12)	5	13.1	37.9
HT(11 > 10)	3	13.4	59.1	HT(12 > 13)	3	13.6	63.1
HT(10 > 9)	3	12.5	64.6	HT(13 > 14)	3	13.1	59.8
HT(9 > 8)	3	13.4	59.1	HT(14 > 15)	4	12.9	55.3
HT(8 > 7)	4	13.4	62.3	HT(15 > 16)	4	12.9	53.4
HT(7 > 6)	4	13.1	58.8	HT(16 > 1)	4	13.0	60.3
HT(6 > 5)	4	13.4	64.9	HT(1 > 2)	3	13.3	56.4
HT(5 > 4)	3	13.3	56.0	HT(2 > 3)	4	10.6	67.6
HT(4 > 3)	4	12.9	56.0	HT(3 > 4)	3	13.5	61.7
HT(3 > 2)	3	13.6	63.3				
HT(2 > 1)	3	13.4	60.4				
HT(1 > 14)	4	13.3	63.5				
HT(14 > 13)	4	13.5	64.7				
HT(13 > 12)	3	13.3	54.8				

slowest, and that between two bonded carbon atoms is the intermediate.

3.2. ATA. *3.2.1. Formation of Radicals.* In order to study the changes in formation energies of radicals and energy barriers of hydrogen transfer reactions with molecular sizes, we calculated the hydrogen transfer reactions of ATA, which has a molecular weight about twice PHE, as summarized in Figure 7. Among these radicals, the radicals of armchair sites including ATA-11-yl and ATA-12-yl are the most stable ones with population probabilities at about 14.8%, while all the other radicals possess similar formation energies with population probabilities at about 5%. Therefore, the radicals of armchair sites are the most abundant ones and armchair edges are dominant growth edges during CVI.

3.2.2. Hydrogen Transfer Pathways and Transition States. The activation energies of hydrogen transfer pathways show similar variations compared with the PHE radicals: the hydrogen transfer pathway between two armchair site carbon atoms, HT(11 > 12), possesses the lowest energy barrier at 29.28 kcal mol^{-1}, and that between two corner site bonded carbon atoms HT(10 > 9) and the two zigzag site carbon atoms HT(5 > 6) and HT(13 > 14), and the highest energy barrier above 60 kcal mol^{-1}. The hydrogen transfer pathways between two corner site carbon atoms of one zigzag site and one bridge site has slightly lower energy barrier than that between two zigzag site carbon atoms. All these transition states have energy barriers between 51 and 61 kcal mol^{-1}.

The structures of the transition states of ATA are similar to the corresponding transition states of PHE as show in Figure 3. For the ATA-TS(11≠12) transition state with two armchair sites, the two C−H bond distances are nearly symmetrical at 1.438 and 1.444 Å; for the ATA-TS(10≠9) transition state with two corner sites, the two C−H bond distances are at 1.334 and 1.335 Å, and for the ATA-TS(4≠3) transition state with two zigzag sites, the two C−H bond distances have the largest values at 1.487 and 1.502 Å.

3.2.3. Hydrogen Transfer Reaction Rate Constants. The hydrogen transfer reaction rate constants of ATA are shown in Figure 8. The reaction rate constants obey the Arrhenius activation process with excellent linear relationship between logarithm of rate constants and the reciprocal of temperature. From the activation energies and pre-exponential factors as shown in Table 2, it could be seen that the activation energies are similar to the energy barriers of the hydrogen transfer pathways, although similar to that of PHE.

3.3. DBP and BNP. In order to study the characteristics of bay site radicals, a few radicals as well as some related hydrogen transfer pathways of the DBP and BNP are studied (Figure 9). The bay site radicals of DBP and BNP possess lower formation energy compared with other radicals because of the absence of steric repulsion, which exists between the two bay site hydrogen atoms in the normal molecules. From our calculations, the formation energies of the bay site radicals DBP-12-yl and DBP-11-yl are 45.75 and 45.51 kcal mol^{-1}, and those of the zigzag site radicals DBP-2-yl and DBP-3-yl are 53.16 and 53.34 kcal mol^{-1}, for about 7.62 kcal mol^{-1} higher than the bay site radicals. For BNP radicals, the bay site radicals BNP-13-yl and BNP-14-yl possess formation of 45.86 and 45.53 kcal mol^{-1}, respectively, almost the same as the DBP radicals.

Compared with the PHE and the ATA, the DBP and the BNP possess bay site configurations and thus steric repulsion between two bay site hydrogen atoms. In order to release the steric repulsion energy, both molecules of DBP and BNP are twisted at the bay sites resulting nonplanar structures. However, all the bay site radicals possess coplanar structure because of the absence of steric repulsion compared with the nonradical normal molecules.

The hydrogen atom transfers easily from one bay site to the other bay site owing to the extremely low energy barrier. For example, the hydrogen transfer energy barrier of DBP-HT(11 > 12) or DBP-HT(12 > 11) is negligible at 4.19 or 3.95 kcal mol^{-1}, and thus the hydrogen transfer reaction is almost spontaneous. For the BNP, similar energy barrier is observed for the hydrogen transfer between two bay site carbon atoms. It is interesting that the hydrogen atom could transfer between carbon atoms 12 and 14 in the BNP radicals, where the two carbon atoms are separated by five carbon atoms. From the geometrical structure of the corresponding transition state BNP-TS(12 ≠ 14) (not shown), it could be seen that BNP-TS(12 ≠ 14) is nonplanar and carbon atoms 12 and 14 are proximal in space, thus the hydrogen atom could transfer between these two carbon atoms. However, the energy barriers

dx.doi.org/10.1021/jp503872m | J. Phys. Chem. A 2014, 118, 4405−4414

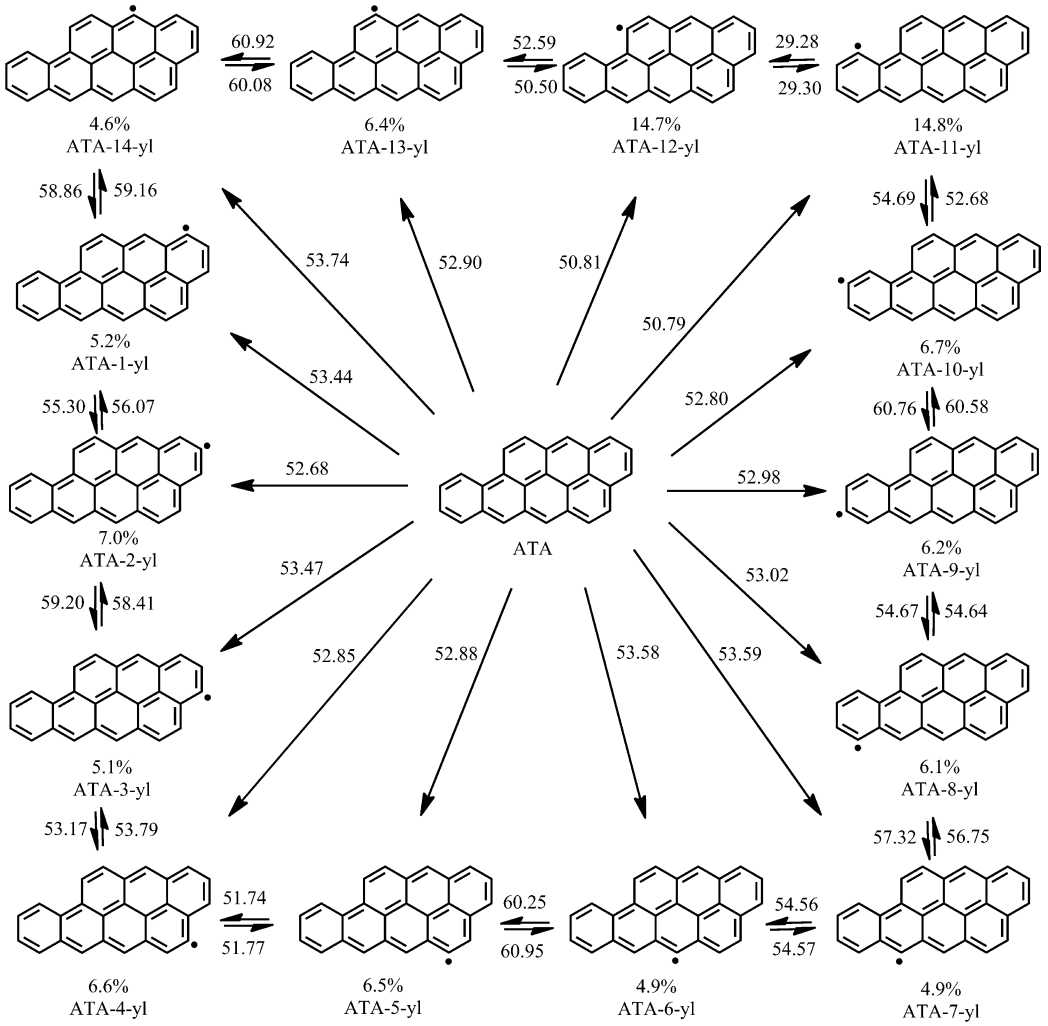

Figure 7. Formation of radicals and the hydrogen transfer pathways of ATA (the meaning of symbols are the same as in Figure 2).

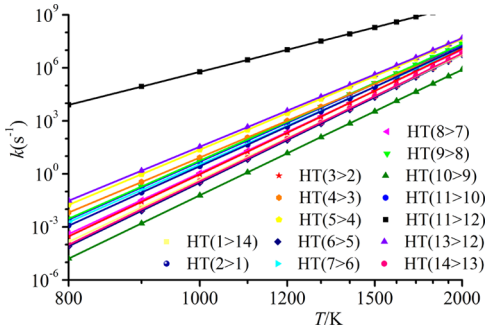

Figure 8. Hydrogen transfer reaction rate constants of ATA.

of hydrogen transfer reaction BNP-HT(12 > 14) and BNP-HT(14 > 12) are nonequivalent with values at 64.42 and 71.84 kcal mol^{-1}, respectively.

The hydrogen transfer reaction rate constants of DBP and BNP are shown in Figure 10 and the activation energies and preexponential factor are summarized in Table 2. It could be seen that rate constants for hydrogen transfer reaction between bay site carbon atoms are much greater than those between armchair carbon atoms and between other carbon atoms.

3.4. DBO. *3.4.1. Hydrogen Transfer Pathways and Transition States.* The formation energy of radical and energy barrier of hydrogen transfer reaction in radical calculated from DFT calculation may be dependent on the size of the model molecule. In this section, we are going to study the formation energies of radicals and the hydrogen transfer pathways of another model molecule DBO, which possesses ten more carbon atoms than ATA. In DBO, the formation energies of radicals of armchair sites are 2.07 kcal mol^{-1} lower on average than the other radicals as shown in Figure 11, almost the same compared with those of ATA. From these calculations, it could be concluded that the formation energy of radicals calculated from DFT converges at even PHE, and the energy difference between a radical at armchair site is about 2.0 kcal mol^{-1} lower than the radicals at other sites.

The hydrogen transfer energy barrier between two armchair carbon atoms is 33.65 kcal mol^{-1}, compared with those between other sites ranging from 49.47 to 63.72 kcal mol^{-1}. These values are consistent with those of PHE and ATA.

The structures of transition states are also very similar between DBO and the other model molecules with C−H distance at about 1.326 and 1.507 Å for the radicals of zigzag sites and armchair sites, respectively (Figure 3).

3.4.2. Hydrogen Transfer Reaction Rate Constants. The hydrogen transfer reaction rate constants fit well to the Arrhenius activation process (Figure 12). The lowest activation energy is observed for hydrogen transfer between two armchair

dx.doi.org/10.1021/jp503872m | J. Phys. Chem. A 2014, 118, 4405−4414

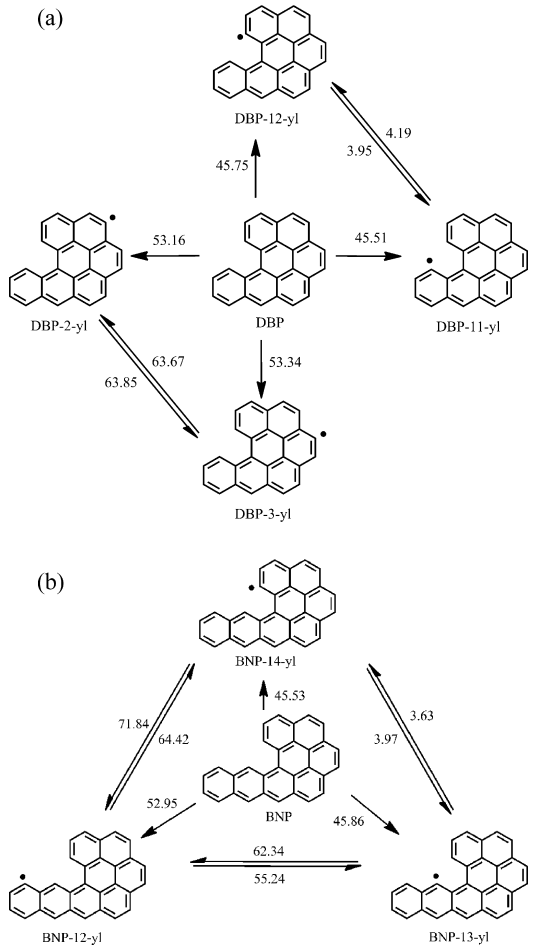

Figure 9. Formation of radicals and hydrogen transfer pathways of (a) DBP and (b) BNP (the meaning of symbols are the same as in Figure 2).

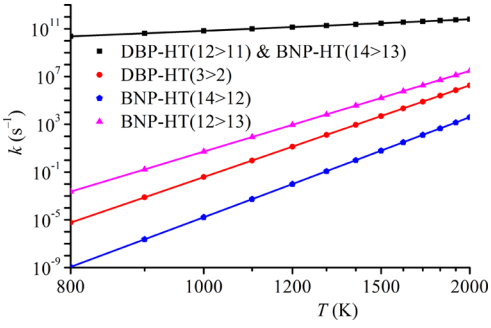

Figure 10. Hydrogen transfer reaction rate constants of DBP and BNP.

sites and the highest between two zigzag sites as shown in Table 2.

4. DISCUSSION AND CONCLUSIONS

The formation energies of radicals and hydrogen transfer pathways of polycyclic aromatic hydrocarbon radicals between various sites are studied using DFT calculations and RRKM/TST calculations, and their influences to the structure of pyrolytic carbon are discussed. The formation energy decreases from radicals of zigzag sites, to radicals of armchair sites and bay sites attributing to the elimination of steric repulsion in the

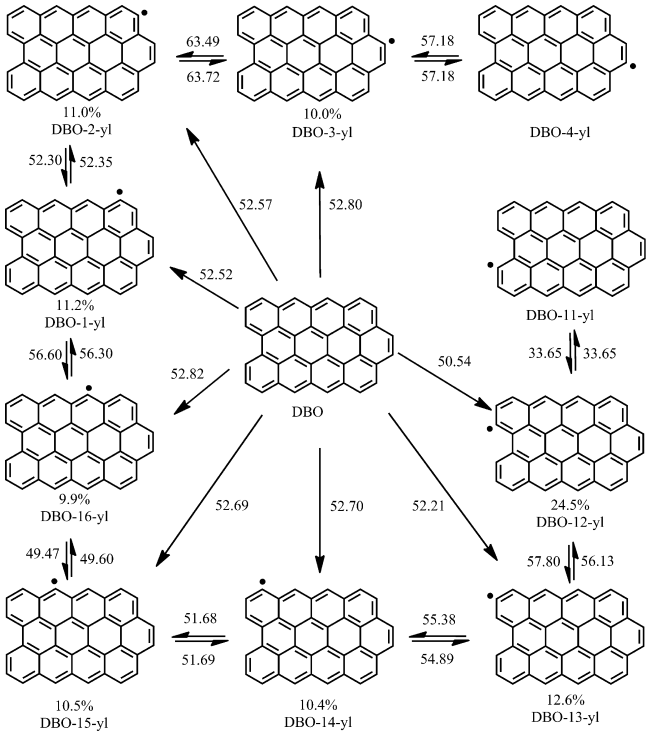

Figure 11. Formation of radicals and hydrogen transfer pathways of DBO (the meaning of the symbols are the same as in Figure 2).

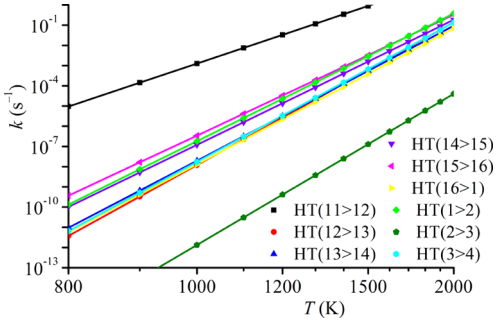

Figure 12. Hydrogen transfer reaction rate constants of DBO.

radicals which exists between the vicinity hydrogen atoms in the normal molecules.

The energy barriers along hydrogen transfer pathways between various sites show systematic changes. For hydrogen transfer between two bay site carbon atoms, the energy barriers are negligible at about 4.0 kcal mol^{-1}. In fact, the corresponding transition states for such hydrogen transfer pathways form six-membered rings, and six-membered ring are believed to be stable in organic chemistry because of the absent of distortion (the members-in-ring of the transition states are summarized in Table 2). For hydrogen transfer between two armchair site carbon atoms, the energy barriers are at intermediate at about 30.0 kcal mol^{-1}. Their corresponding transition states form five-membered rings and the five-membered rings are believed to be similar to the six-membered rings. For hydrogen transfer between two zigzag site carbon atoms and two bonded carbon atoms, the energy barriers are the highest at about 50 kcal mol^{-1}. The transition states for these two cases form four-membered and three-membered rings, and these rings are unstable because of distortion.

dx.doi.org/10.1021/jp503872m | J. Phys. Chem. A 2014, 118, 4405−4414

The transition states of hydrogen transfer between two bonded carbon atoms are nonplanar, while the others are coplanar. For hydrogen transfer pathway with nonplanar transition states, the transferring hydrogen atoms will leave the molecular planes as leaving the initial site for the final site. For all the other hydrogen transfer pathways, the transferring hydrogen atoms will always transport on the molecular planes.

The reaction rate constants fit well to the Arrhenius activation process with a temperature correction parameter of 0.5 and activation energies close to the energy barrier of the transition states.

■ ASSOCIATED CONTENT

Supporting Information

Table SI-1, self-consistent field energy (E_{SCF}), zero-point energy (E_{ZPE}), total energy (E_T), total enthalpy (H_T), and total Gibbs free energy (G_T) at 298.15 K evaluated at the B3LYP/6-311+G(D,P) level of theory (units: Hartree); Table SI-2, high-pressure hydrogen transfer reaction rate constant (s^{-1}) of the PHE radicals using the RRKM/TST approach; Table SI-3, high-pressure hydrogen transfer reaction rate constant (s^{-1}) of the ATA radicals using the RRKM/TST approach; Table SI-4, high-pressure hydrogen transfer reaction rate constant (s^{-1}) of the DBP and BNP radicals using the RRKM/TST approach; Table SI-5, high-pressure hydrogen transfer reaction rate constant (s^{-1}) of the DBO radicals using the RRKM/TST approach. This material is available free of charge via the Internet at http://pubs.acs.org.

■ AUTHOR INFORMATION

Corresponding Author

*E-mail: liuming.yan@shu.edu.cn. Tel: 8621-66132405. Fax: 8621-66132405.

Notes

The authors declare no competing financial interest.

■ ACKNOWLEDGMENTS

The authors thank the financial support from the Chinese National Science Foundation (Grants 21073118 and 21376147), the Innovation Program of Shanghai Municipal Education Commission (Grant 13ZZ078), and the 085 Knowledge Innovation Program, and they acknowledge the High Performance Computing Center and Laboratory for Microstructures, Shanghai University, for computing and structural characterization support.

■ REFERENCES

(1) Awasthi, S.; Wood, J. L. C/C Composite Materials for Aircraft Brakes. *Adv. Ceram. Mater.* **1988**, *3*, 449−451.

(2) Windhorst, T.; Blount, G. Carbon-Carbon Composites: A Summary of Recent Developments and Applications. *Mater. Des.* **1997**, *18*, 11−15.

(3) Huttinger, K. J.; Rosenblatt, U. Pyrolysis Behavior of Coal-Tar and Petroleum Pitches under Pressure. *Carbon* **1975**, *13*, 546−546.

(4) Huttinger, K. J.; Rosenblatt, U. Kinetics of Graphitization-Induced Dimensional Changes of Artificial Carbons. *Carbon* **1975**, *13*, 557−557.

(5) Luo, W.; Fu, Y.; Zhang, S.; Li, H.; Cheng, J.; Xue, L. Thermal Expansion Behaviors of Unidirectional Carbon/Carbon Composites from 800 to 2500 °C. *Ceram. Int.* **2014**, *40*, 6319−6323.

(6) Sheehan, J. E.; Buesking, K. W.; Sullivan, B. J. Carbon-Carbon Composites. *Annu. Rev. Mater. Sci.* **1994**, *24*, 19−44.

(7) Gu, Q.; Kettunen, P. Carbon-Carbon Composite. *Mater. Sci. Eng., A* **1997**, *234*−*236*, 223−225.

(8) Dong, G. L.; Hüttinger, K. J. Consideration of Reaction Mechanisms Leading to Pyrolytic Carbon of Different Textures. *Carbon* **2002**, *40*, 2515−2528.

(9) Bansal, D.; Pillay, S.; Vaidya, U. Nanographite-Reinforced Carbon/Carbon Composites. *Carbon* **2013**, *55*, 233−244.

(10) Cheng, J.; Li, H. J.; Zhang, S. Y.; Xue, L. Z.; Luo, W. F.; Li, W. Failure Behavior Investigation of a Unidirectional Carbon-Carbon Composite. *Mater. Des.* **2014**, *55*, 846−850.

(11) Ziegler, I.; Fournet, R.; Marquaire, P.-M. Influence of Surface on Chemical Kinetic of Pyrocarbon Deposition Obtained by Propane Pyrolysis. *J. Anal. Appl. Pyrolysis* **2005**, *73*, 107−115.

(12) Zhang, W.; Hüttinger, K. Densification of a 2D Carbon Fiber Preform by Isothermal, Isobaric CVI: Kinetics and Carbon Microstructure. *Carbon* **2003**, *41*, 2325−2337.

(13) Tikhomirov, A.; Sorokina, N.; Shornikova, O.; Morozov, V.; Van Tendeloo, G.; Avdeev, V. The Chemical Vapor Infiltration of Exfoliated Graphite to Produce Carbon/Carbon Composites. *Carbon* **2011**, *49*, 147−153.

(14) Zhang, W.; Hu, Z.; Hüttinger, K. Chemical Vapor Infiltration of Carbon Fiber Felt: Optimization of Densification and Carbon Microstructure. *Carbon* **2002**, *40*, 2529−2545.

(15) Lavenac, J.; Langlais, F.; Feron, O.; Naslain, R. Microstructure of the Pyrocarbon Matrix in Carbon/Carbon Composites. *Compos. Sci. Technol.* **2001**, *61*, 339−345.

(16) Becker, A.; Huttinger, K. J. Chemistry and Kinetics of Chemical Vapor Deposition of Pyrocarbon: II. Pyrocarbon Deposition from Ethylene, Acetylene and 1,3-Butadiene in the Low Temperature Regime. *Carbon* **1998**, *36*, 177−199.

(17) Becker, A.; Huttinger, K. J. Chemistry and Kinetics of Chemical Vapor Deposition of Pyrocarbon: III. Pyrocarbon Deposition from Propylene and Benzene in the Low Temperature Regime. *Carbon* **1998**, *36*, 201−211.

(18) Becker, A.; Huttinger, K. J. Chemistry and Kinetics of Chemical Vapor Deposition of Pyrocarbon: IV. Pyrocarbon Deposition from Methane in the Low Temperature Regime. *Carbon* **1998**, *36*, 213−224.

(19) De Pauw, V.; Reznik, B.; Kalhofer, S.; Gerthsen, D.; Hu, Z. J.; Huttinger, K. J. Texture and Nanostructure of Pyrocarbon Layers Deposited on Planar Substrates in a Hot-Wall Reactor. *Carbon* **2003**, *41*, 71−77.

(20) Hu, Z. J.; Huttinger, K. J. Chemistry and Kinetics of Chemical Vapor Deposition of Pyrocarbon: VIII. Carbon Deposition from Methane at Low Pressures. *Carbon* **2001**, *39*, 433−441.

(21) Benzinger, W.; Huttinger, K. J. Chemical Vapor Infiltration of Pyrocarbon: III: The Influence of Increasing Methane Partial Pressure at Increasing Total Pressure on Infiltration Rate and Degree of Pore Filling. *Carbon* **1999**, *37*, 181−193.

(22) Becker, A.; Huttinger, K. J. Chemistry and Kinetics of Chemical Vapor Deposition of Pyrocarbon: V. Influence of Reactor Volume/Deposition Surface Area Ratio. *Carbon* **1998**, *36*, 225−232.

(23) Hu, Z. J.; Zhang, W. G.; Hüttinger, K. J.; Reznik, B.; Gerthsen, D. Influence of Pressure, Temperature and Surface Area/Volume Ratio on the Texture of Pyrolytic Carbon Deposited from Methane. *Carbon* **2003**, *41*, 749−758.

(24) Antes, J.; Hu, Z.; Zhang, W.; Hüttinger, K. Chemistry and Kinetics of Chemical Vapour Deposition of Pyrocarbon: VII. Confirmation of the Influence of the Substrate Surface Area/Reactor Volume Ratio. *Carbon* **1999**, *37*, 2031−2039.

(25) Huttinger, K. J. Cvd in Hot Wall Reactors: The Interaction between Homogeneous Gas-Phase and Heterogeneous Surface Reactions. *Chem. Vap. Deposition* **1998**, *4*, 151−158.

(26) Frenklach, M. Reaction Mechanism of Soot Formation in Flames. *Phys. Chem. Chem. Phys.* **2002**, *4*, 2028−2037.

(27) Ziegler-Devin, I.; Fournet, R.; Lacroix, R.; Marquaire, P. Pyrolysis of Propane for CVI of Pyrocarbon. Part IV: Main Pathways Involved in Pyrocarbon Deposit. *J. Anal. Appl. Pyrolysis* **2013**, *104*, 48−58.

(28) Richter, H.; Howard, J. Formation of Polycyclic Aromatic Hydrocarbons and Their Growth to Soot: A Review of Chemical Reaction Pathways. *Prog. Energy Combust. Sci.* **2000**, *26*, 565−608.
(29) Shukla, B.; Miyoshi, A.; Koshi, M. Role of Methyl Radicals in the Growth of PAHs. *J. Am. Soc. Mass Spectrom.* **2010**, *21*, 534−544.
(30) Li, H.-B.; Page, A. J.; Irle, S.; Morokuma, K. Revealing the Dual Role of Hydrogen for Growth Inhibition and Defect Healing in Polycyclic Aromatic Hydrocarbon Formation: QM/MD Simulations. *J. Phys. Chem. Lett.* **2013**, *4*, 2323−2327.
(31) Wang, Y.; Raj, A.; Chung, S. H. A PAH Growth Mechanism and Synergistic Effect on PAH Formation in Counterflow Diffusion Flames. *Combust. Flame* **2013**, *160*, 1667−1676.
(32) Shukla, B.; Koshi, M. A Highly Efficient Growth Mechanism of Polycyclic Aromatic Hydrocarbons. *Phys. Chem. Chem. Phys.* **2010**, *12*, 2427−2437.
(33) Shukla, B.; Koshi, M. A Novel Route for PAH Growth in HACA Based Mechanisms. *Combust. Flame* **2012**, *159*, 3589−3596.
(34) Bittner, J. D.; Howard, J. B. Composition Profiles and Reaction Mechanisms in a Near-Sooting Premixed Benzene/Oxygen/Argon Flame. In *Eighteenth Symposium (International) on Combustion*; Elsevier: Amsterdam, 1981.
(35) Wang, H.; Frenklach, M. A Detailed Kinetic Modeling Study of Aromatics Formation in Laminar Premixed Acetylene and Ethylene Flames. *Combust. Flame* **1997**, *110*, 173−221.
(36) Kislov, V. V.; Sadovnikov, A. I.; Mebel, A. M. Formation Mechanism of Polycyclic Aromatic Hydrocarbons Beyond the Second Aromatic Ring. *J. Phys. Chem. A* **2013**, *117*, 4794−4816.
(37) Böhm, H.; Jander, H. PAH Formation in Acetylene-Benzene Pyrolysis. *Phys. Chem. Chem. Phys.* **1999**, *1*, 3775−3781.
(38) Ziegler-Devin, I.; Fournet, R.; Marquaire, P.-M. Pyrolysis of Propane for CVI of Pyrocarbon. Part III: Experimental and Modeling Study of the Formation of Pyrocarbon. *J. Anal. Appl. Pyrolysis* **2007**, *79*, 268−277.
(39) Lacroix, R.; Fournet, R.; Ziegler-Devin, I.; Marquaire, P. M. Kinetic Modeling of Surface Reactions Involved in CVI of Pyrocarbon Obtained by Propane Pyrolysis. *Carbon* **2010**, *48*, 132−144.
(40) Xu, P.; Liao, D. M.; Zhou, J. X.; Pang, S. Y. Numerical Simulation of the Influence of Temperature and Pressure in CVI of C/C Composite. *Adv. Mater. Res.* **2012**, *502*, 41−45.
(41) Li, H.; Li, A.; Bai, R.; Li, K. Numerical Simulation of Chemical Vapor Infiltration of Propylene into C/C Composites with Reduced Multi-Step Kinetic Models. *Carbon* **2005**, *43*, 2937−2950.
(42) Wodrich, M. D.; Corminboeuf, C.; Wheeler, S. E. Accurate Thermochemistry of Hydrocarbon Radicals via an Extended Generalized Bond Separation Reaction Scheme. *J. Phys. Chem. A* **2012**, *116*, 3436−3447.
(43) Kislov, V. V.; Mebel, A. M.; Aguilera-Iparraguirre, J.; Green, W. H. Reaction of Phenyl Radical with Propylene as a Possible Source of Indene and Other Polycyclic Aromatic Hydrocarbons: An Ab Initio/RRKM-ME Study. *J. Phys. Chem. A* **2012**, *116*, 4176−4191.
(44) Frisch, M. J.; Trucks, G. W.; Schlegel, H. B.; Scuseria, G. E.; ; Robb, M. A.; Cheeseman, J. R.; Montgomery, J. A.; Vreven Jr., T.; Kudin, K. N.; Burant, J. C.; et al.. *Gaussian 03*, revision C.2; Gaussian, Inc.: Wallingford, CT, 2003.
(45) Cox, J. D.; Wagman, D. D.; Medvedev, V. A. *CAFATA Key Values for Thermodynamics*; Hemisphere Publishing Corp.: New York, 1989.
(46) Mokrushin, V.; Bedanov, V.; Tsang, W.; Zachariah, M.; Knyazev, V. *Chemrate*, version 1.5. 2; National Institute of Standards and Testing: Gaithersburg, MD, 2006.
(47) Norinaga, K.; Deutschmann, O.; Huttinger, K. J. Analysis of Gas Phase Compounds in Chemical Vapor Deposition of Carbon from Light Hydrocarbons. *Carbon* **2006**, *44*, 1790−1800.